


# MCML: Combining physical constraints with experimental data for a multi-purpose meta-generalized gradient approximation

Kristopher Brown<sup>1,2</sup> | Yasheng Maimaiti<sup>1,2</sup> | Kai Trepte<sup>1</sup>  | Thomas Bligaard<sup>3</sup> | Johannes Voss<sup>1</sup> 

<sup>1</sup>SUNCAT Center for Interface Science and Catalysis, SLAC National Accelerator Laboratory, Menlo Park, California, USA

<sup>2</sup>Department of Chemical Engineering, Stanford University, Stanford, California, USA

<sup>3</sup>Department of Energy Conversion and Storage, Technical University of Denmark, Kongens Lyngby, Denmark

## Correspondence

Johannes Voss, SUNCAT Center for Interface Science and Catalysis, SLAC National Accelerator Laboratory, 2575 Sand Hill Road, Menlo Park, CA 94025, USA.  
Email: vossj@slac.stanford.edu

## Funding information

National Defense Science & Engineering Graduate Fellowship (NDSEG); Department of Defense; Chemical Sciences, Geosciences, and Biosciences Division, Catalysis Science Program; Office of Basic Energy Sciences; Office of Science; US Department of Energy

## Abstract

The predictive power of density functional theory for materials properties can be improved without increasing the overall computational complexity by extending the generalized gradient approximation (GGA) for electronic exchange and correlation to density functionals depending on the electronic kinetic energy density in addition to the charge density and its gradient, resulting in a meta-GGA. Here, we propose an empirical meta-GGA model that is based both on physical constraints and on experimental and quantum chemistry reference data. The resulting optimized meta-GGA MCML yields improved surface and gas phase reaction energetics without sacrificing the accuracy of bulk property predictions of existing meta-GGA approaches.

## KEYWORDS

density functional theory, materials predictions, MCML, meta-generalized gradient approximation, surface chemistry

## 1 | INTRODUCTION

Density functional theory (DFT)<sup>1</sup> is used ubiquitously to model the ground-state electronic structure of atoms, molecules, and solids.<sup>2</sup> In the Kohn-Sham approach to DFT,<sup>3</sup> an auxiliary system of single-particle-like equations is solved to obtain the non-interacting kinetic energy of the electrons, and only the average, electrostatic (Hartree) electronic interaction is explicitly computed. An exchange-correlation (XC) functional of the charge density is used to correct for these approximations, yielding the ground-state density and energy of the true, interacting system. The exact form of the XC functional is unknown. Semi-local approximations that only depend on the charge density and, in addition, on its spatial derivatives or on the electronic kinetic energy density at each point in space lead to a particularly efficient approach to model ground-state electronic structures. Depending on the implementation of the diagonalization of the single-particle-like Kohn-Sham Hamiltonian, the complexity of semi-local approximations is at most cubic in system size. The development of semi-local XC functionals enabling electronic structure calculations

of several physical and chemical properties with good accuracy at this relatively low computational cost made DFT one of the most widespread approaches to simulation of electronic structure to date.

Generalized gradient approximations (GGA)<sup>4-10</sup> improve upon a homogeneous electron gas-based local density approximation (LDA)<sup>3,11,12</sup> of the XC functional through density gradient-based corrections. GGA XC functionals can be formulated to be particularly accurate for predictions for some materials properties at the price of deteriorating other predictions. Changing, for example, the low density gradient behavior of the widely used PBE<sup>10</sup> functional to recover the density gradient expansion of the exchange energy of an electron gas in a weak external potential<sup>13</sup> (resulting in the PBEsol functional), lattice constant and bulk elastic property predictions are improved, but the description of solid cohesive energies is worsened in comparison to PBE.<sup>14</sup> Similarly, empirical modifications of PBE (in form of the RPBE and revPBE functionals) improve the description of chemisorption energetics<sup>15,16</sup> while sacrificing the accuracy of lattice constants and bulk elastic properties.<sup>17</sup>

In meta-generalized gradient approximations (meta-GGA),<sup>18-24</sup> additional semi-local quantities such as the Laplacian of the density or

the Kohn-Sham kinetic energy density are used to parameterize the XC functional. In particular, the kinetic energy density can be employed to deduce local chemical bonding character,<sup>22,25</sup> allowing for meta-GGA XC functionals that simultaneously yield accurate lattice constants and solid cohesive energies.<sup>23,24</sup> Meta-GGA XC functionals can furthermore be optimized to yield improved surface adsorption energetics without sacrificing lattice properties.<sup>17,26,27</sup>

For the development of one of the most recent meta-GGAs, SCAN,<sup>24</sup> all 17 known exact constraints and norms of a semi-local functional for model systems with analytical solutions and limiting cases<sup>28</sup> were used, leading to improved thermodynamic stability predictions<sup>29</sup> and to excellent bulk structures and elastic properties for several material classes.<sup>30,31</sup> Chemisorption energetics on transition metal surfaces are, however, predicted less accurately than with several other GGA and meta-GGA approaches, with SCAN generally predicting too strong chemisorption.<sup>27,32,33</sup>

Here, we propose a multi-purpose, constrained, and machine learned (MCML) meta-GGA model that integrates data-driven approaches<sup>17,26,34,35</sup> using experimental and quantum chemistry reference energetics and structures with constraints on the meta-GGA functional form obeying analytical results for model systems, with good simultaneous performance for several materials property predictions through the former and physicality and transferability of the XC model through the latter.

## 2 | METHOD

### 2.1 | Meta-GGA functional optimization

#### 2.1.1 | Exchange functional form

Atomic units  $\hbar = m_e = e = 1$  are used in this section. In a meta-GGA, the exchange energy is typically expressed as an integral of the Dirac exchange energy density of the uniform electron gas (UEG)  $\epsilon_x^{\text{UEG}}[\rho(\mathbf{r})] = -\frac{3}{4}(3/\pi)^{1/3}\rho^{4/3}$  multiplied by an exchange enhancement factor  $F_x(s(\mathbf{r}), \alpha(\mathbf{r}))$

$$E_x[\rho(\mathbf{r})] = \int d^3r F_x(s(\mathbf{r}), \alpha(\mathbf{r})) \cdot \epsilon_x^{\text{UEG}}[\rho(\mathbf{r})], \quad (1)$$

where  $s(\mathbf{r}) = |\nabla\rho(\mathbf{r})|/(2k_F(\mathbf{r})\rho(\mathbf{r}))$  is the reduced density gradient,  $\rho(\mathbf{r})$  is the electronic charge density at  $\mathbf{r}$ , and  $k_F(\mathbf{r}) = \sqrt[3]{3\pi^2\rho(\mathbf{r})}$  is the Fermi wave vector. In the presence of spin polarization, the exchange energy is obtained via spin scaling<sup>36</sup> and evaluating Equation (1) for the individual spin densities. The electronic kinetic energy dependence of meta-GGAs can be parameterized as

$$\alpha(\mathbf{r}) = \frac{\tau^{\text{KS}}(\mathbf{r}) - \tau^{\text{Weizsäcker}}(\mathbf{r})}{\tau^{\text{UEG}}(\mathbf{r})}, \quad (2)$$

where  $\tau^{\text{KS}} = \sum_i n_i |\nabla\phi_i(\mathbf{r})|^2/2$  is the kinetic energy density computed from the Kohn-Sham orbitals  $\phi_i(\mathbf{r})$  with occupation  $n_i$ ,

$\tau^{\text{Weizsäcker}}(\mathbf{r}) = |\nabla\rho(\mathbf{r})|^2/(8\rho(\mathbf{r}))$ , and  $\tau^{\text{UEG}}(\mathbf{r}) = \frac{3}{10}(3\pi^2)^{2/3}\rho(\mathbf{r})^{5/3}$  is the non-interacting kinetic energy density of a UEG with charge density equal to  $\rho(\mathbf{r})$ .  $\tau^{\text{Weizsäcker}}(\mathbf{r})$  vanishes for zero charge density gradient and equals  $\tau^{\text{KS}}(\mathbf{r})$  for a density composed of a single (singly or doubly occupied) orbital. Equation (2) thus approaches zero in the single orbital limit and one in the homogeneous limit with  $\nabla\rho(\mathbf{r})=0$  and  $\tau^{\text{KS}}(\mathbf{r}) = \tau^{\text{UEG}}(\mathbf{r})$ . With that, the parameter  $\alpha$  can be used to locally detect the type of bonding and optimize the exchange enhancement for these different bonding scenarios.<sup>22,25</sup>

As a starting point for the data-driven meta-GGA development, we employ the MS2 meta-GGA functional.<sup>23</sup> As will be shown in Section 3, this functional exhibits relatively good accuracy for bulk and surface reaction energetics. The MS2 exchange enhancement factor can be expressed as an  $\alpha$ -weighted sum of two GGA exchange enhancement factors:

$$F_x^{\text{MS2}}(s(\mathbf{r}), \alpha(\mathbf{r})) = \{1 - \hat{\alpha}(\mathbf{r})\} \left( 1 + \kappa_{\text{MS2}} - \frac{\kappa_{\text{MS2}}^2}{\kappa_{\text{MS2}} + \mu^{\text{GE}} s^2(\mathbf{r})} \right) + \hat{\alpha}(\mathbf{r}) \left( 1 + \kappa_{\text{MS2}} - \frac{\kappa_{\text{MS2}}^2}{\kappa_{\text{MS2}} + \mu^{\text{GE}} s^2(\mathbf{r}) + C_{\text{MS2}}} \right), \quad (3)$$

with the weighting function

$$\hat{\alpha}(\mathbf{r}) = \frac{(1 - \alpha^2(\mathbf{r}))^3}{1 + \alpha^3(\mathbf{r}) + 4\alpha^6(\mathbf{r})}. \quad (4)$$

The maximum value of  $F_x^{\text{MS2}}$  is  $1 + \kappa_{\text{MS2}} = 1.504$ .  $\mu^{\text{GE}} = 10/81$  is the lowest-order coefficient of the gradient correction to the free electron gas exchange energy.<sup>13</sup> The coefficient  $C_{\text{MS2}} = 0.14601$  ensures that the hydrogen atom Hartree energy is canceled.

The correlation part of MS2 is a GGA, that is, the correlation functional does not depend on the parameter  $\alpha$ .<sup>21,22</sup> We optimize the exchange enhancement factor as described in the following, but keep the correlation functional fixed at the MS2 form.

Following Lundgaard et al.<sup>17</sup> and Wellendorff et al.,<sup>26</sup> we choose an expansion of the exchange enhancement  $F_x(s(\mathbf{r}), \alpha(\mathbf{r}))$  in Legendre polynomials  $P_i(\hat{s})$  and  $P_j(\hat{\alpha})$  for numerical optimization

$$F_x(s(\mathbf{r}), \alpha(\mathbf{r})) = \sum_{i=0}^7 \sum_{j=0}^7 c_{ij} P_i(\hat{s}(\mathbf{r})) P_j(\hat{\alpha}(\mathbf{r})), \quad (5)$$

where

$$\hat{s}(\mathbf{r}) = \frac{2s^2(\mathbf{r})}{\eta + s^2(\mathbf{r})} - 1 \quad (6)$$

maps the semi-infinite interval  $[0, \infty]$  of possible reduced density gradients to the Legendre polynomial domain  $[-1, 1]$ . Here,  $\eta = \kappa/\mu^{\text{GE}}$  is chosen such that the exchange enhancement of PBEsol<sup>14</sup> can be

expressed by the first two Legendre polynomials  $P_0(\hat{s}(r))$  and  $P_1(\hat{s}(r))$ ;  $1 + \kappa = 1.804$  is the local Lieb–Oxford bound.<sup>37,38</sup> Similarly, we use  $\hat{\alpha}(r)$ , which is equal to the MS2 weighting function (4), to map the semi-infinite interval of possible values for  $\alpha(r)$ .

We approximate the MS2 exchange enhancement (3) to  $10^{-7}$  relative precision by the polynomial expansion (5). The corresponding expansion coefficients  $c_{ij}^{\text{MS2}}$  can be found in the Supporting Information, Appendix S3, and we use these coefficients as an initial guess for the exchange enhancement factor optimization. The MS2 exchange enhancement fulfills three equality constraints from physical models.<sup>22</sup> We constrain the optimization to not deviate from these analytical solutions as described in the following.

## 2.1.2 | Physical constraints

Of the 64 coefficients  $c_{ij}$  determining our exchange enhancement approximation, Equation (5), three are eliminated through linear equations for analytical constraints. First, for  $s = 0$  and  $\alpha = 1$  the UEG limit is recovered with an enhancement of 1:

$$\sum_{i=0}^7 \sum_{k=0}^3 (-1)^{i+k} \frac{(2k)!}{2^{2k}(k!)^2} c_{i,2k} = 1. \quad (7)$$

Second, the exchange gradient expansion, of importance for prediction of lattice properties,<sup>14</sup> is recovered with a curvature of  $2\mu^{\text{GE}}$  in  $s$  around zero at  $\alpha = 1$

$$\sum_{i=0}^7 \sum_{k=0}^3 -(-1)^{i+k} \frac{(2k)!}{2^{2k}(k!)^2} \frac{2i(i+1)}{\eta} c_{i,2k} = 2\mu^{\text{GE}}. \quad (8)$$

Third, the spurious Hartree energy of the hydrogen atom (single orbital density:  $\alpha = 0$ ) of 0.3125 Hartree is canceled

$$\sum_{i=0}^7 \sum_{j=0}^7 \int_0^\infty dr r^2 \frac{-3 \cdot 6^{1/3}}{\pi^{2/3}} \exp(-8r/3) \times P_i(\hat{s}^{\text{H}}(r)) c_{ij} = -0.3125, \quad (9)$$

with  $\hat{s}^{\text{H}}(r) = p^{\text{H}}(r) / [\eta + p^{\text{H}}(r)] - 1$ , and  $p^{\text{H}}(r) = (6\pi)^{-2/3} \exp(4r/3)$  is the square of the reduced density gradient of the 1s hydrogen atom ground state. The integrals appearing in Equation (9) are evaluated numerically,<sup>39</sup> leading to a numerically exact constraint for single-orbital systems.

The  $\sim s^{-1/2}$  decay of the exchange enhancement for large reduced density gradients  $s$  is not introduced into our exchange enhancement expansion, Equation (5). This decay is only known to be an exact constraint for  $\alpha = 0$ ,<sup>28</sup> and the reduced gradients computed for the benchmark systems studied here (see Section 2.3) do not cover large enough  $s$  and  $\alpha$  ranges to empirically determine decay constants (if any) for  $\alpha > 0$  ( $s$  becomes large in exponentially decaying density tails, but the Dirac exchange energy is proportional to  $\rho^{4/3}$  and thus the contribution to  $E^{\text{x}}[\rho]$  is vanishing exponentially in these regions). With the most important ranges of reduced gradients  $s \lesssim 10$ ,

the expansion is limited to seventh order Legendre polynomials. Much larger gradients occurring in the vicinity of nuclei do not explicitly appear in our simulations, as these are frozen in the employed pseudopotentials (see Section 2.2), which are generated from PBE all-electron atomic orbitals. The usage of such PBE pseudopotentials is common practice for pseudopotential meta-GGA calculations due to the (current) lack of meta-GGA pseudopotentials.<sup>29,32</sup>

## 2.1.3 | Exchange functional fitting

The remaining 61 degrees of freedom in the exchange enhancement, Equation (5), are fitted to quantum chemistry and experimental reference data (described in Section 2.3), minimizing the errors for predicting reaction and cohesive energies, lattice constants, and bulk moduli. A reaction energy at  $T = 0$  K for reactants  $\mathcal{R}$  and products  $\mathcal{P}$  can be computed from DFT total energies as

$$E^{\text{react}} = \sum_{i \in \mathcal{P}} p_i E_i - \sum_{j \in \mathcal{R}} q_j E_j, \quad (10)$$

where  $p_i$  and  $q_j$  are prefactors accounting for the stoichiometry of products and reactants in the reaction, respectively, and  $E_i$  and  $E_j$  are the corresponding DFT total energies for the respective species.

Here, all atomic structures and total energies are determined first using the MS2 meta-GGA. Estimates for reaction energies with a different exchange functional are obtained non-self-consistently by evaluating this functional on the fixed atomic structures and charge densities as obtained with the MS2 functional

$$E_{\text{estimate}}^{\text{react}} = E_{\text{MS2}}^{\text{react}} - \left( \sum_{i \in \mathcal{P}} p_i E_{\text{MS2}i}^{\text{x}} - \sum_{j \in \mathcal{R}} q_j E_{\text{MS2}j}^{\text{x}} \right) + \sum_{i \in \mathcal{P}} p_i E_i^{\text{x}} - \sum_{j \in \mathcal{R}} q_j E_j^{\text{x}}, \quad (11)$$

where  $E_{\text{MS2}i}^{\text{x}}$  and  $E_{\text{MS2}j}^{\text{x}}$  are the exchange energies of products and reactants as computed self-consistently with the MS2 functional, and  $E_i^{\text{x}}$  and  $E_j^{\text{x}}$  are computed non-self-consistently using the exchange enhancement of Equation (5). Given the charge density  $\rho_k(\mathbf{r})$  determined using the MS2 functional for a system  $k \in \mathcal{P} \cup \mathcal{R}$ , the estimated exchange energy is

$$E_k^{\text{x}} = \sum_{i=0}^7 \sum_{j=0}^7 c_{ij}^k I_{ij}^k, \quad (12)$$

with the 64 volume integrals

$$I_{ij}^k = \int d^3r P_i(\hat{s}(\mathbf{r})) P_j(\hat{\alpha}(\mathbf{r})) \times c_{\text{x}}^{\text{UEG}}[\rho_k(\mathbf{r})]. \quad (13)$$

Keeping the densities of all considered systems fixed at their MS2-based densities during the optimization of the  $c_{ij}$ , the evaluation

of the exchange energy estimates requires minimal computational effort, as the integrals in Equation (13) only need to be evaluated once per system.

The above strategy for generating a  $c_{ij}$ -parameterized estimate for the exchange component of reaction energies allows for the efficient prediction of the error for data sets such as cohesive energy and chemisorption data sets. This can be further extended to bulk moduli and lattice constants, which can be approximated as weighted sums of total energies  $\sum_i w_i E_i$ . With the total energy  $E_{\text{eq}}$  of a solid at equilibrium unit cell volume  $V_{\text{eq}}$  and total energies  $E_\nu$  at unit cell volumes  $V_\nu = V_{\text{eq}} + \nu \cdot \Delta V$ , the bulk modulus  $K$  is approximated here as  $K_{\text{fit}}$  using a five point stencil at constant volume spacing  $\Delta V$

$$K_{\text{fit}} = V_{\text{eq}} \times \frac{-E_{-2} + 16E_{-1} - 30E_{\text{eq}} + 16E_{+1} - E_{+2}}{12(\Delta V)^2}. \quad (14)$$

The lattice constant or, equivalently, the optimum unit cell volume is approximated as  $V_{\text{fit}}$ , defined to be the minimum of a parabola through the three volumes  $V_{\pm 1}$  and  $V_{\text{eq}}$

$$V_{\text{fit}} = -\frac{V_{\text{eq}}}{2(\Delta V)^2 K_{\text{MS2}}} \times ((-2V_{\text{eq}} - \Delta V)E_{-1} + 4V_{\text{eq}}E_{\text{eq}} + (-2V_{\text{eq}} + \Delta V)E_{+1}), \quad (15)$$

where  $K_{\text{MS2}}$  is the bulk modulus obtained with the MS2 functional. Non-self-consistent estimates of bulk moduli and optimum cell volumes in dependence of the coefficients  $c_{ij}$  are obtained in analogy to Equation (11) by subtracting the MS2 exchange energies from the total energies  $E_{\text{eq}}$ ,  $E_{\pm 1, \pm 2}$  and adding the corresponding exchange energies according to Equation (12). Equations (11), (14), and (15) are linear in the coefficients  $c_{ij}$ , allowing for efficient evaluation and optimization of the corresponding predictions as described in the following.

To simultaneously optimize bulk structures, bulk moduli and reaction energetics, the following product error is employed:

$$\text{Loss}'(\theta) = \prod_i \left( \sum_{d \in D_i} \left( R_d^{\text{ref}} - R_d^{\text{predict}}(\theta) \right)^2 \right)^{\gamma_i}, \quad (16)$$

where  $\theta$  is a 61-dimensional vector representing the remaining degrees of freedom for the coefficients  $c_{ij}$ , eliminating the constraints Equations (7)–(9).  $R_d^{\text{ref}}$  are the fitting target reference data, and  $R_d^{\text{predict}}(\theta)$  are the fitted, non-self-consistent DFT predictions computed using Equations (11), (14), and (15) for reaction energies, bulk moduli, and equilibrium unit cell volumes, respectively. The powers  $\gamma_i$  are weights for the data sets  $D_i$  in the product error. Different units of the optimized properties and different sizes of the benchmark data sets  $D_i$  merely lead to a prefactor of the overall product error.

Due to lack of data in the DFT benchmark calculations for  $\alpha \rightarrow \infty, s \rightarrow \infty$ , the fit is stabilized by adding a penalty for the

enhancement factor to deviate from the local Lieb-Oxford bound of 1.804 for  $\alpha \rightarrow \infty, s \rightarrow \infty$

$$\text{Loss}(\theta) = \text{Loss}'(\theta) + \beta(1.804 - F_x(\theta; s \rightarrow \infty, \alpha \rightarrow \infty))^2. \quad (17)$$

The penalty weight  $\beta$  is chosen here as  $\text{Loss}'(\text{MS2})/60$ , where  $\text{Loss}'(\text{MS2})$  is the product error of DFT predictions using the MS2 functional. We find this relatively small penalty to stabilize the fit in keeping the exchange enhancement factor bound for all  $s, \alpha$  without forcing it to approach the local Lieb-Oxford bound exactly (the exchange enhancement of the optimized MCML meta-GGA indeed remains below the bound with a maximum value of  $F_x \approx 1.4$  at  $s \approx 2.4$  and  $\alpha = 0$ ).

Starting from the MS2 exchange enhancement factor as an initial guess (fulfilling all physical constraints considered here), Equation (17) is minimized using the Nelder–Mead simplex algorithm.<sup>40–42</sup> This procedure could be repeated iteratively, recomputing atomic structures and charge densities with the fitted XC functional instead of MS2. Such re-iterations were not considered here, as we have found the fitted functional to already perform well on re-optimized atomic structures and energetics after one fitting iteration.

## 2.2 | Electronic structure calculations

DFT calculations are performed using projector-augmented wave pseudopotentials<sup>43,44</sup> to represent ionic cores and expanding the Kohn-Sham states in plane wave basis sets as implemented in the Vienna ab initio Simulation Package (VASP).<sup>45</sup> The basis sets are cut off at kinetic energies as described in Section 2.3, with particularly high cutoff energies for bulk systems to minimize spurious Pulay stress and thus to reduce lattice constant errors. Atomic structures are optimized until the maximum force acting on any ion is at most 0.02 eV/Å. Brillouin zones are sampled using Gaussian smearing with a width of 0.05 eV and  $k$ -point grids (3D grids for bulk systems and 2D grids for slabs) with a maximum spacing of  $0.02 \text{ \AA}^{-1}$ .

## 2.3 | Benchmark data sets

The reference data described in the following consists of bulk properties as well as surface and gas phase reaction energetics. This wide variety ensures a range of applicability for material property predictions of the optimized meta-GGA. The systems contained in each data set with MCML predictions and comparisons to MS2, SCAN, mBEEF, and PBE can be found in the Supporting Information, Appendices S1 (overview of reactions) and S6 (DFT predictions).

### 1. Surface-phase data

- ADS41 (reactions listed in Table S5): The ADS41 data set<sup>32</sup> originates from high-precision experimental data (equilibrium adsorption studies, temperature programmed desorption, and single crystal adsorption calorimetry), which were zero-point

energy corrected.<sup>46</sup> We split this data set into chemisorption-dominated systems (called CHEMI26) and dispersion-dominated systems (called DISP15) so that these properties can be separately evaluated and optimized. Surfaces are modeled with slabs consisting of four metal layers separated by at least  $\sim 15$  Å of vacuum to avoid spurious interactions between periodic images of the slabs. A plane wave cutoff of 700 eV is used. Two bottom metallic layers are fixed at their bulk positions, while the two topmost layers and adsorbate atoms are relaxed.

## 2. Gas-phase data

- DBH24 (reactions listed in Table S1): This data set contains 12 forward and 12 reverse gas phase reaction barrier heights, as described in Zheng et al.<sup>47</sup> These reference values come from the quadratic configuration interaction with single and double excitations (QCISD) wavefunction method. These values are compared to total energy differences between single-point calculations (i.e., no structural relaxation) at a plane wave cutoff of 800 eV in supercells with  $\sim 25$  Å spacing between periodic images of the species.
- S66x8 (systems listed in Table S3): The S66x8 set consists of non-covalent interactions (a balance of dispersion and electrostatic interactions) for 66 molecular complexes at 8 distances, as described in Rezc et al.<sup>48</sup> These reference values are compared to total energy differences of single-point calculations using a 700 eV plane wave cutoff in supercells with  $\sim 24$  Å spacing.
- RE42 (reactions listed in Table S4): This set contains 42 gas-phase reaction energies at 0 K involving 45 molecules from the G3/99 set, compiled in Wellendorff et al.<sup>35</sup> and based on Pople et al.<sup>49</sup> and Curtiss et al.<sup>50</sup> Molecular structures are relaxed at a 700 eV plane wave cutoff in supercells with  $\sim 20$  Å spacing, and differences between total energies are compared to the reference values found in Wellendorff et al.<sup>35</sup>
- W4-11 (molecules listed in Tables S6–S7): This data set contains 140 atomization energies of small molecules, with

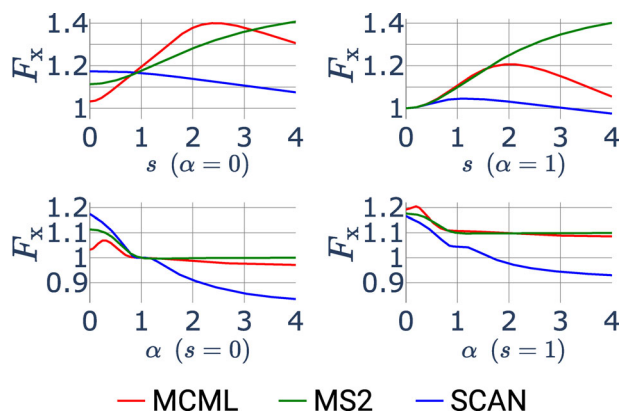


**FIGURE 1** MCML exchange enhancement factor, varied along the reduced density gradient  $s$  (top) and the kinetic energy density parameter  $\alpha$  (bottom) with projections along  $\alpha$  and  $s$ , respectively, at values of 0 and 1. In comparison, the exchange enhancement factors of the MS2 and SCAN functionals are shown

reference values computed from first principles using the Weizmann-4 computational thermochemistry method.<sup>51</sup> Here, single-point calculations are performed with a 800 eV plane wave cutoff in supercells with 25 Å spacing. This data set is purely used for testing.

- BH-76 (reactions listed in Table S8): This data set contains 76 gas phase barriers. It appeared as a subset of the GMTKN30

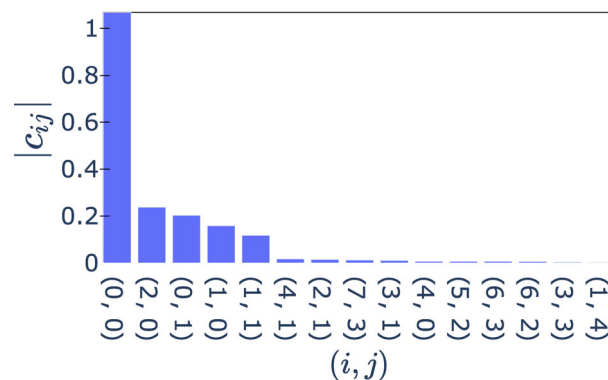


**FIGURE 2** The 15 coefficients in  $c_{ij}$  of largest magnitude versus the indices  $(i, j)$  of the exchange enhancement expansion (3). There are five major contributions which all come from low-degree polynomials

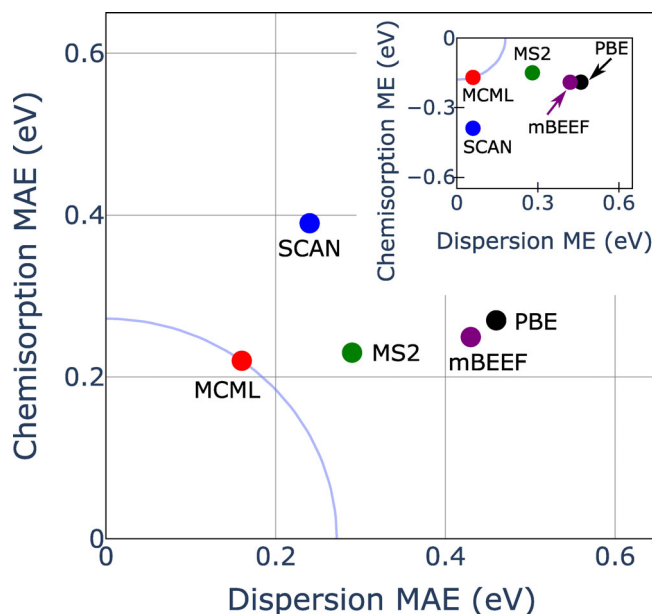


**FIGURE 3** Mean absolute error MAE of predictions using several XC functionals for dispersion-dominated adsorption (DISP15) versus chemisorption (CHEMI26) on transition metal surfaces. The inset shows the corresponding mean (signed; positive: underbinding, negative: overbinding) error, ME. Only semi-local DFT approaches are compared here, and besides mBEEF and PBE only functionals fulfilling all three constraints described in Section 2.1.2 are considered. MCML shows here the best performance both for chemisorption and physisorption as indicated by the quadrant in the lower left corner of the plot. SCAN, MS2, and PBE data from Mallikarjun Sharada et al.<sup>32</sup>

Data set	Unit	Metric	MCML	MS2	SCAN	mBEEF	PBE
CHEMI26	eV	MAE	0.22	0.23	0.39	0.25	0.27
		RMSE	0.26	0.27	0.45	0.30	0.31
		ME	-0.17	-0.15	-0.39	-0.19	-0.19
DISP15	eV	MAE	0.16	0.29	0.24	0.43	0.46
		RMSE	0.18	0.33	0.28	0.51	0.52
		ME	0.06	0.28	0.06	0.42	0.46
DBH24	eV	MAE	0.26	0.27	0.31	0.24	0.35
		RMSE	0.32	0.31	0.36	0.27	0.45
		ME	-0.26	-0.26	-0.31	-0.22	-0.35
RE42	eV	MAE	0.28	0.42	0.34	0.23	0.32
		RMSE	0.43	0.54	0.47	0.29	0.45
		ME	0.10	-0.08	-0.11	-0.04	-0.09
S66x8	eV	MAE	0.023	0.050	0.033	0.028	0.067
		RMSE	0.033	0.068	0.043	0.045	0.099
		ME	0.016	0.048	0.033	0.012	0.067
W4-11	eV	MAE	0.43	0.33	0.18	0.16	0.59
		RMSE	0.60	0.49	0.23	0.22	0.73
		ME	-0.32	-0.23	-0.10	-0.10	0.52
BH-76	eV	MAE	0.30	0.29	0.34	0.26	0.40
		RMSE	0.37	0.36	0.38	0.30	0.47
		ME	-0.29	-0.29	-0.33	-0.25	-0.40
CE65	eV	MAE	0.23	0.21	0.20	0.22	0.18
		RMSE	0.32	0.31	0.30	0.33	0.25
		ME	-0.01	0.09	-0.07	-0.12	-0.05
BM64	GPa	MAE	9.4	10.2	9.6	10.3	12.6
		RMSE	16.1	17.9	16.1	16.4	16.2
		ME	5.3	7.7	5.7	3.1	-7.7
LP68	Å	MAE	0.033	0.032	0.033	0.040	0.060
		RMSE	0.044	0.042	0.044	0.052	0.077
		ME	0.012	0.008	0.011	0.016	0.056

**TABLE 1** Functional performance on surface, gas, and bulk phase data sets

Note: The metrics used are mean absolute error (MAE), root mean square error (RMSE), and mean error (ME). Positive ME indicates predicted values greater than target values, on average. CHEMI26 and DISP15 data for MS2, SCAN, and PBE from Mallikarjun Sharada et al.<sup>32</sup>

database,<sup>52</sup> with data originally from Zhao et al.<sup>53,54</sup> Here, single-point calculations are performed with a 800 eV plane wave cutoff in supercells with 25 Å spacing. The reactions in this data set include the 24 barriers in DBH24. The data in BH-76 are purely used for testing.

### 3. Solid-phase data (systems listed in Table S2)

- All bulk calculations are run with a 1000 eV plane wave cutoff. Using zero-point energy corrections from a Debye model,<sup>55</sup> experimental data for bulk cohesive energies, lattice constants, and bulk moduli are used as benchmarks. Instead of expressing bulk moduli and lattice constants via the stencil-based expressions required for optimizing the exchange enhancement in terms of exchange energy contributions, Equations (14) and (15), the final, self-consistent evaluation of these bulk

properties is performed via over-determined equation of states fits.<sup>55,56</sup> The evaluation is furthermore extended to bulk reference data as benchmarked in Zhang et al.<sup>30</sup> in addition to the bulk training data from Wellendorff et al.<sup>26,35</sup> and Hao et al.<sup>57</sup> as described in the following:

- CE65: 65 solid cohesive energies for metallic and binary compounds are the union of reference data collected in Wellendorff et al.<sup>26</sup> and Zhang et al.<sup>30</sup> The heaviest element considered in the data sets is Au, as heavier elements such as Pb typically exhibit large errors in predicted cohesive energies.<sup>30,35</sup>
- CE65\_sub: a subset of CE65 consisting of the cohesive energies of Pd, W, Ta, Pt, Ir, Cu, and Sn. Separating these seven materials with relatively high errors in predicted cohesive energies<sup>30,35</sup> allows for them to have a lower weighting in the fitting

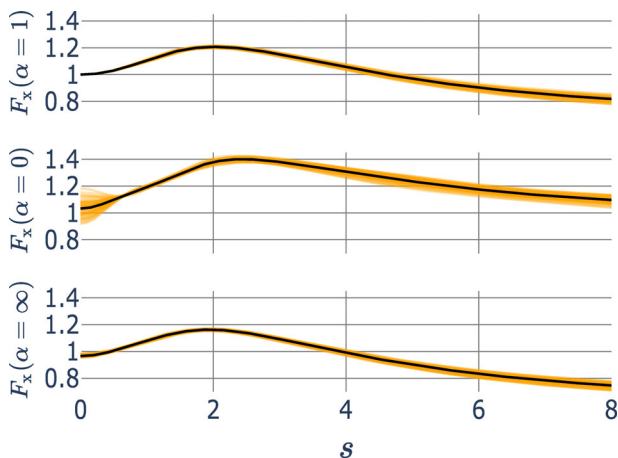


**FIGURE 4** Bayesian ensemble of exchange enhancement factors as perturbations of MCML. There is larger spread in the ensemble at larger values of  $s$  (where there is not an abundance of training data). There is no uncertainty in the UEG limit ( $s=0$ ,  $\alpha=1$ ), where the model is exactly constrained

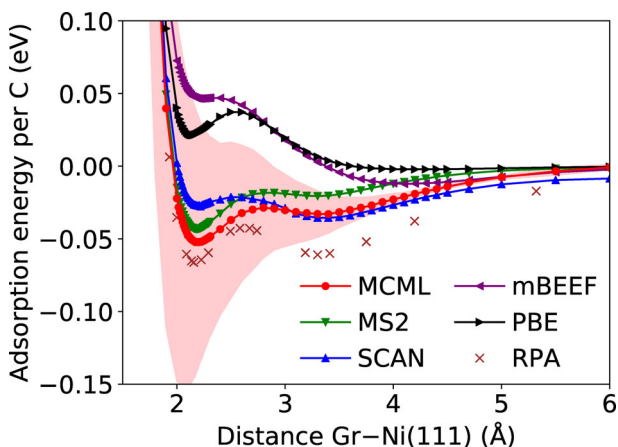


**FIGURE 5** Adsorption energy as a function of distance of graphene in top-fcc configuration on Ni(111). Random phase approximation (RPA) data at fixed RPA-optimized bulk lattice spacing from Mittendorfer et al.<sup>58</sup> For comparison, the DFT calculations are performed without Ni-surface layer relaxation at XC functional-dependent, optimized bulk lattice constants. MCML qualitatively correctly predicts a chemisorption minimum and a weaker physisorption minimum at larger distance. The shaded area corresponds to  $\pm 1$  SD computed from a Bayesian ensemble of 5000 perturbations to the MCML exchange enhancement

procedure than the remaining solid training data corresponding to lower cohesive energy errors (weights applied to training data can be found in the Supporting Information, Appendix S6).

- LP68: Union of the lattice constant reference data presented in Zhang et al.<sup>30</sup> and Hao et al.<sup>57</sup> with zero-point corrected experimental values. Like above, the heaviest element considered is Au.
- BM64: Union of bulk modulus reference data from Zhang et al.<sup>30</sup> and Wellendorff et al.<sup>35</sup> This data set contains 64 bulk

moduli for elemental and binary compounds with Au being the heaviest element considered.

## 3 | RESULTS AND DISCUSSION

### 3.1 | The optimized MCML meta-GGA

By minimizing the cost function, Equation (17), a new exchange enhancement factor was found which was then benchmarked self-consistently by re-optimizing atomic structures and re-computing electronic charge densities. The resulting exchange enhancement is controlled by the weighting powers  $\gamma_i$  on the data sets  $D_i$ . We find that atoms have larger deviations in the self-consistently computed exchange energies from the non-self-consistently computed values on MS2 charge densities than solids. For the considered atoms, the mean absolute deviation is here  $\sim 0.22$  eV, while for the solids it is  $\sim 0.03$  eV per atom. Due to the resulting sensitivity of bulk cohesive energies, we use a high weighting power of 5 for all cohesive energies but the systems in CE65\_sub with generally large errors. CE65\_sub and all remaining data sets are weighted with powers of 1. The goal of this weighting is to emphasize cohesive energies in general but not to overemphasize outliers.

The resulting compromise of minimizing residual prediction errors for the data sets  $D_i$  yields the MCML exchange enhancement factor (see Figure 1). For  $\alpha=1$ , the functional shape of MCML is very similar to MS2, but the MCML exchange enhancement factor decays for large  $s$  in contrast to MS2, which is monotonously increasing. While the decaying behavior renders MCML here qualitatively similar to SCAN, the SCAN exchange enhancement is generally much lower for large  $s$  than the enhancement of MCML.

The numerical coefficients (Appendix S2) and FORTRAN code (Appendix S4) for evaluating the exchange part of the functional can be found in the Supporting Information. Of the 61 fitting degrees of freedom, only five coefficients for low polynomial orders have major contributions to the exchange enhancement factor (Figure 2). For these five dominant  $c_{ij}$  the maximum Legendre polynomial order in  $\hat{s}$  is 2, while in  $\hat{a}$  it is only 1. Accordingly, the functional form of the MCML exchange enhancement is relatively smooth.

### 3.2 | Comparison to other XC functionals

To assess the quality of the predictions using the MCML functional presented here, we perform a comparison to four other XC functionals: PBE, mBEEF, MS2, and SCAN. While MCML, MS2, and SCAN obey all three constraints considered here, PBE only obeys constraint (7). mBEEF violates all three constraints: the UEG limit (7) is overshoot by  $\sim 3.7\%$ , the curvature limit (8) is  $\sim 21.7\%$  too small, and the hydrogen atom self-interaction correction (9) is too negative by  $\sim 0.22$  eV. First, we present a comparison of the performance for chemisorption and physisorption on transition metal surfaces, the accurate prediction of which is particularly important for the field of heterogeneous catalysis (Figure 3).

Of the semi-local XC functionals considered here, MCML shows the lowest absolute errors both for physisorption and chemisorption. MCML neither exhibits consistent over- nor under-binding for dispersion and only slight overbinding for chemisorption on average.

In addition to improving the surface data sets, MCML significantly improves predictions for reaction energies between gas phase molecular species (RE42 and S66x8: see Table 1). For gas phase reaction barriers (DBH24 and BH-76) MS2 and MCML show very similar errors (MCML, MS2, SCAN, mBEEF, and PBE predictions for all considered bulk, surface, and gas phase systems are listed with the benchmark targets in the Supporting Information, Appendix S6). Low errors for molecular atomization energies (W4-11) and also for gas phase reaction barriers are found for mBEEF. MCML performs worse than the other meta-GGAs for W4-11 but better than PBE. MCML furthermore shows an 0.02 eV increase in mean absolute error for the CE65 data set in comparison to the starting guess of MS2. While MCML shows improvements for surface-adsorbate and molecule-molecule reaction energies, atomization energies of molecules and solids are thus not improved.

mBEEF shows an improvement in lattice constant predictions over PBE, but it performs worse than all other considered meta-GGAs. The lattice constant improvement over PBE is achieved, although the constraint (8) recovering the exchange gradient expansion of importance for good description of lattice constants<sup>14</sup> is violated by mBEEF. The violation of the constraints (7), (8), and (9), despite generally good performance on the benchmark data, could thus indicate a potentially unphysical mBEEF meta-GGA model.

MCML lattice constant and bulk modulus predictions are on average as accurate as those from the SCAN functional (see Table 1). Accordingly, MCML constitutes a multi-purpose meta-GGA functional with improved surface and gas phase reaction energetics without sacrificing the description of bulk properties.

### 3.3 | Bayesian uncertainty analysis

In addition to enabling the computationally efficient exchange enhancement factor optimization presented here, the decomposition of the exchange energy into a weighted sum over 64 volume integrals shown in Equation (12) also allows for efficient Bayesian estimation of errors in the exchange energy due to uncertainty in the exchange enhancement factor.<sup>17,26,34,35</sup> With a cost function  $\text{Loss}_2(\theta)$  yielding the squared error against data set  $D$  of predictions using the exchange enhancement factor model  $M$  with model parameters  $\theta$ , a probability distribution for  $\theta$  can be defined as  $P(\theta|MD) \propto \exp(-\text{Loss}_2(\theta)/\tau)$ , where  $\tau$  is a fictitious temperature.<sup>34</sup> In the vicinity of least-square optimal parameters  $\theta_0$  minimizing the cost function,  $\text{Loss}_2(\theta)$  is approximately quadratic and can thus be approximated by a second order Taylor expansion. Then, a distribution of exchange enhancement model parameters can be defined as introduced in Mortensen et al.<sup>34</sup> and summarized here as  $\theta = \theta_0 + U\Lambda^{-1/2}\nu$ , where  $\nu$  is a 61-dimensional vector with unit width Gaussian distributed components for the exchange enhancement model  $M$  considered

here.  $U$  is an orthogonal matrix composed column-wise of the eigenvectors of the Hessian  $\mathcal{H}$  of  $\text{Loss}_2$  at  $\theta_0$ , and  $\Lambda$  is a diagonal matrix such that  $\mathcal{H}/\tau = U\Lambda U^T$ .

The parameters  $\theta^{\text{MCML}}$  minimize the penalized product error cost function, Equation (17), rather than a least-squares cost function. To enable the above generation of ensembles of exchange enhancement factors, we define an auxiliary least-squares cost function  $\text{Loss}_2^{\text{aux}}(\theta) = \frac{1}{2} \sum_i \sum_{d \in D_i} \left[ R_d^{\text{ref}} - R_d^{\text{predict}}(\theta) \right]^2 / \mathcal{N}_i + \frac{1}{2} \theta^T \Theta \theta$ , where  $\mathcal{N}_i = \sum_{d \in D_i} \left[ R_d^{\text{ref}} - R_d^{\text{predict}}(\theta^{\text{MCML}}) \right]^2$  is used to normalize the different data sets  $D_i$  accounting both for different units and numbers of systems in the sets. In analogy to Wellendorff et al.,<sup>35</sup>  $\frac{1}{2} \theta^T \Theta \theta$  is a regularizing term. Here, we choose the matrix  $\Theta$  such that  $\theta^{\text{MCML}}$  is a least squares optimum of  $\text{Loss}_2^{\text{aux}}(\theta)$ , with  $\Theta = 2 \mid \lambda_{\min} \mid \Omega$ .  $\Omega$  is the projector onto the space spanned by eigenvectors with eigenvalues  $\leq 0$  of the Hessian  $\mathcal{H}_0$  of  $\text{Loss}_2^{\text{aux}}$  for  $\Theta = 0$ , and  $\lambda_{\min}$  is the smallest of the eigenvalues. The resulting cost function Hessian  $\mathcal{H}_0 + \Theta$  has thus only positive eigenvalues. The fictitious temperature  $\tau$  is chosen such that the variance of predicted reaction energies, lattice constants and bulk moduli computed with an ensemble of exchange enhancement factors coincides with the mean-squared error given by the MCML XC functional for  $\text{Loss}_2^{\text{aux}}$  (numerical values for all matrices including computer source code required to compute ensembles of such perturbations of MCML can be found in the Supporting Information, Appendix S5).

An ensemble of perturbations of the MCML exchange enhancement factor can be used to non-self-consistently estimate the uncertainty in the MCML exchange energy and, correspondingly, in quantities such as total energy differences. Here, we use such an ensemble to analyze uncertainty in the exchange enhancement factor given the training benchmark data and model in form of the expansion shown in Equation (5) (see Figure 4). For low reduced density gradients  $s \leq 5$ , which are typical values for metals and for which there are an abundance of training data in the benchmark calculations, there is generally less uncertainty in the exchange enhancement than at larger  $s$ , with the exception of the single-orbital  $\alpha = 0$  limit at vanishing  $s$ , where there is particularly high uncertainty. These regions of high uncertainty also correspond to  $s, \alpha$  parameter ranges where there exists large variation between established functionals such as MS2 and SCAN.

As an example for the prediction of uncertainties on reaction energetics, we compare the adsorption energy for graphene on Ni(111) in top-fcc configuration as computed with the MCML, MS2, SCAN, mBEEF, and PBE functionals to random phase approximation (RPA) results.<sup>58</sup> As the adsorption energetics as a function of distance between graphene and Ni surface are sensitive to the lattice constants,<sup>59</sup> we perform these DFT simulations at a plane wave cutoff of 1000 eV. For comparison to the computationally expensive RPA simulations at fixed RPA-optimized bulk lattice spacing of Ni, we employ the functional-dependent, optimized lattice constants of Ni (values in the Supporting Information, Appendix S6), but do not allow any atoms to relax their positions as the distance between graphene and five fixed layers of Ni is varied. Of the considered functionals, MCML shows least deviation from the RPA results, predicting chemisorption that is stronger than a second physisorption minimum at

larger distance (Figure 5). None of the considered functionals predict binding of graphene as strong as predicted within the RPA, where the RPA is likely underestimating the chemisorption strength.<sup>60</sup> mBEEF predicts a particularly shallow unbound local chemisorption minimum with a depth of only  $\sim 1$  meV. Supplementing semi-local DFT with non-local correlation (which will be considered in future empirical meta-GGA work) leads to stronger binding of graphene on Ni(111).<sup>59</sup> The shaded area in Figure 5 shows  $\pm 1$  SD as computed using a Bayesian ensemble of 5000 perturbations to the MCML exchange enhancement. The predicted uncertainty vanishes at large distances, due to almost complete error cancellation between graphene and Ni-slab with vanishing mutual interaction in the same supercell with respect to the two reactants in separate supercells. The predicted uncertainty is relatively large in the vicinity of the chemisorption minimum, where even the PBE unbound local energy minimum falls into 1 SD from MCML. The spread of the MCML perturbations is chosen such that it reproduces a least-squares fitting error for all considered reference data sets  $D_i$ , and the uncertainty predictions shown in Figure 5 are consistent with the root mean square errors of 0.26 and 0.18 eV for the CHEMI26 and DISP15 surface chemistry data sets, respectively.

It should be noted that MCML is a locally optimal solution to the non-linear optimization problem of minimizing the penalized product error cost function, Equation (17), starting from MS2 as an initial guess. Furthermore, larger exchange enhancement model spaces (e.g., through inclusion of higher-order Legendre polynomials in Equation (5) or of exponential factors similar to the SCAN functional) can lead to optimal exchange enhancement factors that are not covered by the spread of the ensemble shown in Figure 4. Estimation of errors on DFT total energetic predictions using the ensemble will generally only be useful if the systems studied are described relatively well by semi-local DFT. If semi-local DFT fundamentally fails in describing the electronic structure, Bayesian error estimates based on the MCML ensemble will generally not yield the large error in predictions for such systems.

## 4 | CONCLUSION

MCML is an empirical meta-GGA functional optimized with bulk, surface, and gas phase quantum chemistry and experimental benchmark data while simultaneously obeying physical constraints, leading to a multi-purpose XC functional. Improvements are achieved for surface and gas phase reaction energetics without sacrificing the good performance of existing meta-GGA functionals for bulk structural and elastic properties. Although MCML already shows relatively good performance for dispersion-dominated properties, extending the combined data and physical constraint based approach to non-local functionals explicitly describing van der Waals interactions will be the subject of future work, where both exchange enhancement and non-local correlations are going to be re-parameterized simultaneously for an overall improvement of performance for a range of physical and chemical properties.

## ACKNOWLEDGMENTS

This research was supported by the US Department of Energy, Office of Science, Office of Basic Energy Sciences, Chemical Sciences,

Geosciences, and Biosciences Division, Catalysis Science Program to the SUNCAT Center for Interface Science and Catalysis. K. B. acknowledges support by the Department of Defense (DoD) through the National Defense Science & Engineering Graduate Fellowship (NDSEG) Program.

## DATA AVAILABILITY STATEMENT

In addition to data available in the supplementary material of this article, further data supporting the findings of this study are available from the corresponding author upon reasonable request.

## ORCID

Kai Trepte  <https://orcid.org/0000-0003-2214-2467>

Johannes Voss  <https://orcid.org/0000-0001-7740-8811>

## REFERENCES

- [1] P. Hohenberg, W. Kohn, *Phys. Rev.* **1964**, *136*, B864.
- [2] W. Kohn, A. D. Becke, R. G. Parr, *J. Phys. Chem.* **1996**, *100*, 12974.
- [3] W. Kohn, L. J. Sham, *Phys. Rev.* **1965**, *140*, A1133.
- [4] D. C. Langreth, J. P. Perdew, *Phys. Rev. B* **1980**, *21*, 5469.
- [5] D. C. Langreth, M. J. Mehl, *Phys. Rev. B* **1983**, *28*, 1809.
- [6] J. P. Perdew, *Phys. Rev. Lett.* **1965**, *1985*, 55.
- [7] J. P. Perdew, W. Yue, *Phys. Rev. B* **1986**, *33*, 8800.
- [8] A. D. Becke, *Phys. Rev. A* **1988**, *38*, 3098.
- [9] C. Lee, W. Yang, R. G. Parr, *Phys. Rev. B* **1988**, *37*, 785.
- [10] J. P. Perdew, K. Burke, M. Ernzerhof, *Phys. Rev. Lett.* **1996**, *77*, 3865.
- [11] D. M. Ceperley, B. J. Alder, *Phys. Rev. Lett.* **1980**, *45*, 566.
- [12] J. P. Perdew, Y. Wang, *Phys. Rev. B* **1992**, *45*, 13244.
- [13] P. R. Antoniewicz, L. Kleinman, *Phys. Rev. B* **1985**, *31*, 6779.
- [14] J. P. Perdew, A. Ruzsinszky, G. I. Csonka, O. A. Vydrov, G. E. Scuseria, L. A. Constantin, X. Zhou, K. Burke, *Phys. Rev. Lett.* **2008**, *100*, 136406.
- [15] B. Hammer, L. B. Hansen, J. K. Nørskov, *Phys. Rev. B* **1999**, *59*, 7413.
- [16] Y. Zhang, W. Yang, *Phys. Rev. Lett.* **1998**, *80*, 890.
- [17] K. T. Lundgaard, J. Wellendorff, J. Voss, K. W. Jacobsen, T. Bligaard, *Phys. Rev. B* **2016**, *93*, 235162.
- [18] J. Tao, J. P. Perdew, V. N. Staroverov, G. E. Scuseria, *Phys. Rev. Lett.* **2003**, *91*, 146401.
- [19] Y. Zhao, D. G. Truhlar, *J. Chem. Phys.* **2006**, *125*, 194101.
- [20] A. D. Becke, E. R. Johnson, *J. Chem. Phys.* **2006**, *124*, 221101.
- [21] J. P. Perdew, A. Ruzsinszky, G. I. Csonka, L. A. Constantin, J. Sun, *Phys. Rev. Lett.* **2009**, *103*, 026403.
- [22] J. Sun, B. Xiao, A. Ruzsinszky, *J. Chem. Phys.* **2012**, *137*, 051101.
- [23] J. Sun, R. Haunschild, B. Xiao, I. W. Bulik, G. E. Scuseria, J. P. Perdew, *J. Chem. Phys.* **2013**, *138*, 044113.
- [24] J. Sun, A. Ruzsinszky, J. P. Perdew, *Phys. Rev. Lett.* **2015**, *115*, 036402.
- [25] J. Sun, B. Xiao, Y. Fang, R. Haunschild, P. Hao, A. Ruzsinszky, G. I. Csonka, G. E. Scuseria, J. P. Perdew, *Phys. Rev. Lett.* **2013**, *111*, 106401.
- [26] J. Wellendorff, K. T. Lundgaard, K. W. Jacobsen, T. Bligaard, *J. Chem. Phys.* **2014**, *140*, 144107.
- [27] E. W. F. Smeets, J. Voss, G.-J. Kroes, *J. Phys. Chem. A* **2019**, *123*, 5395.
- [28] J. P. Perdew, A. Ruzsinszky, J. Sun, K. Burke, *J. Chem. Phys.* **2014**, *140*, 18A533.
- [29] Y. Zhang, D. A. Kitchaev, J. Yang, T. Chen, S. T. Dacek, R. A. Sarmiento-Pérez, M. A. L. Marques, H. Peng, G. Ceder, J. P. Perdew, *J. Sun, NPJ Comput. Mater.* **2018**, *4*, 9.
- [30] G.-X. Zhang, A. M. Reilly, A. Tkatchenko, M. Scheffler, *New J. Phys.* **2018**, *20*, 063020.

- [31] M. Bokdam, J. Lahnsteiner, B. Ramberger, T. Schäfer, G. Kresse, *Phys. Rev. Lett.* **2017**, *119*, 145501.
- [32] S. Mallikarjun Sharada, R. K. B. Karlsson, Y. Maimaiti, J. Voss, T. Bligaard, *Phys. Rev. B* **2019**, *100*, 035439.
- [33] A. Patra, H. Peng, J. Sun, J. P. Perdew, *Phys. Rev. B* **2019**, *100*, 035442.
- [34] J. J. Mortensen, K. Kaasbjerg, S. L. Frederiksen, J. K. Nørskov, J. P. Sethna, K. W. Jacobsen, *Phys. Rev. Lett.* **2005**, *95*, 216401.
- [35] J. Wellendorff, K. T. Lundgaard, A. Møgelhøj, V. Petzold, D. D. Landis, J. K. Nørskov, T. Bligaard, K. W. Jacobsen, *Phys. Rev. B* **2012**, *85*, 235149.
- [36] G. L. Oliver, J. P. Perdew, *Phys. Rev. A* **1979**, *20*, 397.
- [37] E. H. Lieb, S. Oxford, *Int. J. Quantum Chem.* **1981**, *19*, 427.
- [38] J. P. Perdew, in *Unified Theory of Exchange and Correlation Beyond the Local Density Approximation, Electronic Structure of Solids '91* (Eds: P. Ziesche, H. Eschrig), Akademie Verlag, Berlin **1991**, p. 11.
- [39] QUADPACK: FORTRAN subroutine package for the numerical computation of definite one-dimensional integrals, <https://www.netlib.org/quadpack/> (accessed on 27 February 2020).
- [40] J. A. Nelder, R. Mead, *Comput. J.* **1965**, *7*, 308.
- [41] F. Gao, L. Han, *Comput. Optim. Appl.* **2012**, *51*, 259.
- [42] P. Virtanen, R. Gommers, T. E. Oliphant, M. Haberland, T. Reddy, D. Cournapeau, E. Burovski, P. Peterson, W. Weckesser, J. Bright, S. J. van der Walt, M. Brett, J. Wilson, K. J. Millman, N. Mayorov, A. R. J. Nelson, E. Jones, R. Kern, E. Larson, C. J. Carey, İ. Polat, Y. Feng, E. W. Moore, J. VanderPlas, D. Laxalde, J. Perktold, R. Cimrman, I. Henriksen, E. A. Quintero, C. R. Harris, A. M. Archibald, A. H. Ribeiro, F. Pedregosa, P. van Mulbregt, SciPy 1.0 Contributors, A. Vijaykumar, A. P. Bardelli, A. Rothberg, A. Hilboll, A. Kloeckner, A. Scopatz, A. Lee, A. Rokem, C. N. Woods, C. Fulton, C. Masson, C. Häggström, C. Fitzgerald, D. A. Nicholson, D. R. Hagen, D. V. Pasechnik, E. Olivetti, E. Martin, E. Wieser, F. Silva, F. Lenders, F. Wilhelm, G. Young, G. A. Price, G. L. Ingold, G. E. Allen, G. R. Lee, H. Audren, I. Probst, J. P. Dietrich, J. Silterra, J. T. Webber, J. Slavič, J. Nothman, J. Buchner, J. Kulick, J. L. Schönberger, J. V. de Miranda Cardoso, J. Reimer, J. Harrington, J. L. C. Rodríguez, J. Nunez-Iglesias, J. Kuczynski, K. Tritz, M. Thoma, M. Newville, M. Kümmerer, M. Bolingbroke, M. Tartre, M. Pak, N. J. Smith, N. Nowaczyk, N. Shebanov, O. Pavlyk, P. A. Brodtkorb, P. Lee, R. T. McGibbon, R. Feldbauer, S. Lewis, S. Tygier, S. Sievert, S. Vigna, S. Peterson, S. More, T. Pudlik, T. Oshima, T. J. Pingel, T. P. Robitaille, T. Spura, T. R. Jones, T. Cera, T. Leslie, T. Zito, T. Krauss, U. Upadhyay, Y. O. Halchenko, Y. Vázquez-Baeza, *Nat. Methods* **2020**, *17*, 261.
- [43] P. E. Blöchl, *Phys. Rev. B* **1994**, *50*, 17953.
- [44] G. Kresse, D. Joubert, *Phys. Rev. B* **1999**, *59*, 1758.
- [45] G. Kresse, J. Furthmüller, *Phys. Rev. B* **1993**, *54*, 11169.
- [46] J. Wellendorff, T. L. Silbaugh, D. Garcia-Pintos, J. K. Nørskov, T. Bligaard, F. Studt, C. T. Campbell, *Surf. Sci.* **2015**, *640*, 36.
- [47] J. Zheng, Y. Zhao, D. G. Truhlar, *J. Chem. Theory Comput.* **2007**, *3*, 569.
- [48] J. Rezc, K. E. Riley, P. Hobza, *J. Chem. Theory Comput.* **2011**, *7*, 2427.
- [49] J. A. Pople, M. Head-Gordon, D. J. Fox, *J. Chem. Phys.* **1989**, *90*, 5622.
- [50] L. A. Curtiss, K. Raghavachari, J. A. Pople, *J. Chem. Phys.* **1993**, *98*, 1293.
- [51] A. Karton, S. Daon, J. M. Martin, *Chem. Phys. Lett.* **2011**, *510*, 165.
- [52] L. Goerigk, S. Grimme, *J. Chem. Theory Comput.* **2011**, *7*, 291.
- [53] Y. Zhao, B. J. Lynch, D. G. Truhlar, *J. Phys. Chem. A* **2004**, *108*, 2715.
- [54] Y. Zhao, N. González-García, D. G. Truhlar, *J. Phys. Chem. A* **2005**, *109*, 2012.
- [55] A. B. Alchagirov, J. P. Perdew, J. C. Boettger, R. C. Albers, C. Fiolhais, *Phys. Rev. B* **2001**, *63*, 224115.
- [56] A. H. Larsen, J. J. Mortensen, J. Blomqvist, I. E. Castelli, R. Christensen, M. Dułak, J. Friis, M. N. Groves, B. Hammer, C. Hargus, E. D. Hermes, P. C. Jennings, P. B. Jensen, J. Kermode, J. R. Kitchin, E. L. Kolsbjerg, J. Kubal, K. Kaasbjerg, S. Lysgaard, J. B. Maronsson, T. Maxson, T. Olsen, L. Pastewka, A. Peterson, C. Rostgaard, J. Schiøtz, O. Schütt, M. Strange, K. S. Thygesen, T. Vegge, L. Vilhelmsen, M. Walter, Z. Zeng, K. W. Jacobsen, *J. Phys.: Condens. Matter* **2017**, *29*, 273002.
- [57] P. Hao, Y. Fang, J. Sun, G. I. Csonka, P. H. Philipsen, J. P. Perdew, *Phys. Rev. B* **2012**, *85*, 014111.
- [58] F. Mittendorfer, A. Garhofer, J. Redinger, s. š., J. Klime, J. Harl, G. Kresse, *Phys. Rev. B* **2011**, *84*, 201401.
- [59] S. Shepard, M. Smeu, *J. Chem. Phys.* **2019**, *150*, 154702.
- [60] T. Olsen, K. S. Thygesen, *Phys. Rev. B* **2013**, *87*, 075111.

**How to cite this article:** K. Brown, Y. Maimaiti, K. Trepte, T. Bligaard, J. Voss, *J. Comput. Chem.* **2021**, *1*, <https://doi.org/10.1002/jcc.26732>